

Resource usage and gene circuit performance characterization in a cell-free ‘breadboard’

Dan Siegal-Gaskins^{1,*}, Zoltan A. Tuza^{2,*}, Jongmin Kim^{1,*},
Vincent Noireaux³, and Richard M. Murray^{1,4}

1. Division of Biology and Biological Engineering, California Institute of Technology, Pasadena, CA, USA
2. Faculty of Information Technology, Pazmany Peter Catholic University, Budapest, Hungary
3. School of Physics and Astronomy, University of Minnesota, Minneapolis, MN, USA
4. Department of Control and Dynamical Systems, California Institute of Technology, Pasadena, CA, USA

* These authors contributed equally to this work.

Abstract

The many successes of synthetic biology have come in a manner largely different from those in other engineering disciplines; in particular, without well-characterized and simplified prototyping environments to play a role analogous to wind-tunnels in aerodynamics and breadboards in electrical engineering. However, as the complexity of synthetic circuits increases, the benefits—in cost savings and design cycle time—of a more traditional engineering approach can be significant. We have recently developed an *in vitro* ‘breadboard’ prototyping platform based on *E. coli* cell extract that allows biocircuits to operate in an environment considerably simpler than but functionally similar to *in vivo*. The simplicity of the cell-free transcription-translation breadboard makes it a promising tool for rapid biocircuit design and testing, as well as for probing the fundamentals of gene circuit functions that are normally masked by cellular complexity. In this work we characterize the cell-free breadboard using real-time and simultaneous measurements of transcriptional and translational activities of a small set of reporter genes and a transcriptional activation cascade. We determine the effects of promoter strength, gene, and nucleoside triphosphate concentrations on biocircuit properties, and we isolate contributions of the essential components—core RNA polymerase, housekeeping sigma factor, and ribosomes—to overall performance. Importantly, we show how limits on essential resources, particularly those involved in translation, are manifested as reduced expression in the presence of orthogonal genes that serve as additional loads on the system.

Keywords

cell-free systems, biological circuit prototyping, crosstalk, *in vitro* synthetic biology, RNA aptamer

Abbreviations

TX: transcription; TL: translation; FP: fluorescent protein; MGapt: malachite green RNA aptamer; UTR: untranslated region; RNAP: RNA polymerase; NTP: nucleoside triphosphate; RBS: ribosome binding site

Introduction

The field of synthetic biology has matured to the point where biological parts are regularly assembled into modestly complex circuits with wide-ranging applications [1]. Unfortunately, the development of new biological circuits typically involves long and costly *ad hoc* design cycles characterized by trial-and-error and lacking the prototyping stage essential to other engineering disciplines. More often than not, designed circuits fail to operate as expected. The reason for these failures is in many cases related to *context*: the poorly characterized environment in which the system is operating [2–4]. This includes the finite and variable (from cell to cell, condition to condition, and time to time) pools of biomolecular resources such as transcription/translation machinery and nucleoside triphosphates (NTPs), weak control over the component DNA concentrations, unpredicted interactions between components and circuits and their cellular hosts (see, e.g., [5,6]), and any number of other system properties with unknown or unknowable effects.

We have recently developed an *in vitro* biomolecular ‘breadboard’ based on *E. coli* cell extract that provides a functional environment similar to *in vivo* but with significantly reduced complexity [7,8]. DNA and mRNA endogenous to the cells is eliminated during extract preparation, so that transcription-translation circuits of interest may be operated in isolation without interference by a cellular host. The cell-free breadboard also allows for a degree of control over reaction conditions and component concentrations that cannot be achieved *in vivo*. As a prototyping platform, the cell-free breadboard provides for a considerable reduction in circuit design cycle time, not only because of its relative simplicity when compared with *in vivo*, but also because it eliminates much of the lengthy cloning and cell transformation steps typically required in biocircuit development (see, e.g., [9]). Indeed, cell-free applications for synthetic biology are quickly expanding [10,11]. But beyond its potential as an improved circuit development platform, our cell-free breadboard has another significant advantage: its simplicity reveals important details of biocircuit operation normally masked by cellular complexity.

In this work we show a detailed and quantitative characterization of the cell-free breadboard—an essential precursor to any biocircuit development and testing application—and explore a number of fundamental aspects of biocircuit operation not easily studied *in vivo*. Central to our work is the use of a novel reporter that combines the malachite green RNA aptamer and a fluorescent protein for a real-time and simultaneous read-out of the system’s transcription and translation activity. We establish the functional implications of intrinsic biocircuit properties such as component concentration and promoter strength, as well as those of the extrinsic biomolecular resource pool that includes nucleoside triphosphates (NTPs), sigma factors, and other transcription/translation machinery. Finally, through a systematic characterization of the effect of loads on transcriptional and translational performance, we show how limits on essential resources, particularly those involved in translation, manifest themselves in the form of reduced expression and ‘crosstalk’ between orthogonal genes. Implications for biocircuit prototyping are discussed.

Results

To best characterize transcription- and translation-level performance in the cell-free breadboard platform, we use a reporter construct encoding a green or cyan fluorescent protein (deGFP/deCFP) along with the malachite green RNA aptamer (MGapt) in the 3′ untranslated region (UTR) (Fig. 1A). These fluorescent proteins (FPs) have been previously designed and optimized for maximal expression in the cell-free system when transcribed from *E. coli* promoters [7]. The 35-base MGapt sequence contains a binding pocket for the malachite green dye [12] and allows for real-time fluorescence monitoring of RNA dynamics with a temporal resolution significantly higher than what has been previously achieved in cell extract using radio-labeling and gel analysis (e.g., in [13]). The use of MGapt as a measure of RNA was validated using real-time PCR and by comparing deGFP levels with and without the aptamer in the 3′ UTR (Figs. S3 and S4).

that are more sharply-peaked.

Protein expression curves (Fig. 1C) show simpler translation dynamics—protein degradation machinery is absent from the standard cell-free breadboard—but again we see qualitative differences above and below a 2–5 nM DNA threshold. Above, deGFP production slows gradually before stopping at ~ 500 minutes. Below the threshold the profiles may be described as piecewise linear functions with roughly constant positive slope for times $t < t_{end,TL} \approx 350$ minutes and zero slope for $t > t_{end,TL}$. Given that $t_{end,TL}$ appears fixed for all concentrations in this regime, it is unlikely that the cessation of protein production is due to complete consumption of necessary resources by the translation machinery. Similar results have been noted previously [14] with the suggestion that a number of other processes, including NTP hydrolysis and enzyme denaturation, may lead to early termination of protein synthesis reactions [15, 16].

We use two simple measures to better compare transcription- and translation-level performance under different conditions: MGapt integrated over the course of the experiment ($\int_{t=0}^{t_{end}} \text{MGapt}(t') dt' = \int \text{MGapt}$) and the concentration of deGFP at the end of the experiment ($\text{deGFP}(t_{end}) = [\text{deGFP}]_{end}$). The choice of these performance metrics is motivated by the relationship between integrated MGapt and deGFP concentrations under ‘ideal’ conditions: in the absence of protein degradation, and under the naive assumptions of unlimited resources and conditions unchanging with time, a simple model for deGFP production may be written as

$$\frac{d}{dt} \text{deGFP}(t) = k_{TL} \text{MGapt}(t - t_{mat}) \quad (1)$$

for constants k_{TL} and t_{mat} , and thus deGFP at any time t^* may be expected to be proportional to $\int^{t^*} \text{MGapt}$ (with a short delay for deGFP maturation). This model was previously validated for up to one hour of expression [13]. Below the 2–5 nM DNA threshold described above and for times $t < t_{end,TL}$ we find that this proportionality continues to hold true (Fig. 2A), although the relationship between $\text{deGFP}(t^*)$ and $\int^{t^*} \text{MGapt}$ becomes much less straightforward as resources are consumed and system conditions change with time (see Supporting Information). Plotting $\int \text{MGapt}$ and $[\text{deGFP}]_{end}$ as a function of plasmid concentration (Fig. 2B), we see a ‘linear’ regime in which $[\text{deGFP}]_{end}$ is proportional to DNA concentration and a ‘saturation’ regime in which $[\text{deGFP}]_{end}$ versus DNA concentration is sublinear. These regimes correspond to the qualitative differences in the MGapt and deGFP expression curves described above. Surprisingly, we see no significant change in $\int \text{MGapt}$ at the transition between regimes.

Transcription, translation, and promoter strength

To determine how promoter strength affects transcription and translation in our cell-free breadboard, we tested the reporter construct under the control of two additional constitutive promoters Pr1 and Pr2 made weaker than Pr by single base mutations in the -35 and -10 region, respectively (see Materials and Methods). We find that the concentration at which the system transitions from the linear regime to the saturation regime is increased for these weaker promoters, up to ~ 10 nM for Pr1 and ~ 20 nM for Pr2 (Fig. S7). Thus, we see something of a performance trade-off between DNA concentration and promoter strength: a weaker promoter allows for ‘linear’ performance with higher template concentrations.

The overall performance under different promoters can be summarized and compared in a plot of $[\text{deGFP}]_{end}$ versus $\int \text{MGapt}$, effectively a measure of protein produced per transcript (Fig. 3). Worth noting is the dramatic increase in the Pr curve at the regime transition point, an increase not seen for the weaker promoters. This may be explained by the differential transcriptional dynamics in the ‘linear’ and ‘saturation’ regimes—distributed versus peaked—coupled with decreasing activity of the translation machinery. Such a time-dependent reduction in translational efficiency, reported in other cell-free systems [14], would mean that although transcription may take place later in the experiment, the resulting transcripts are less translatable.

What is clear from Fig. 3 is that the relationship between DNA template concentration, promoter strength, integrated RNA, and final protein concentration is not a simple one; for example, with 2 nM

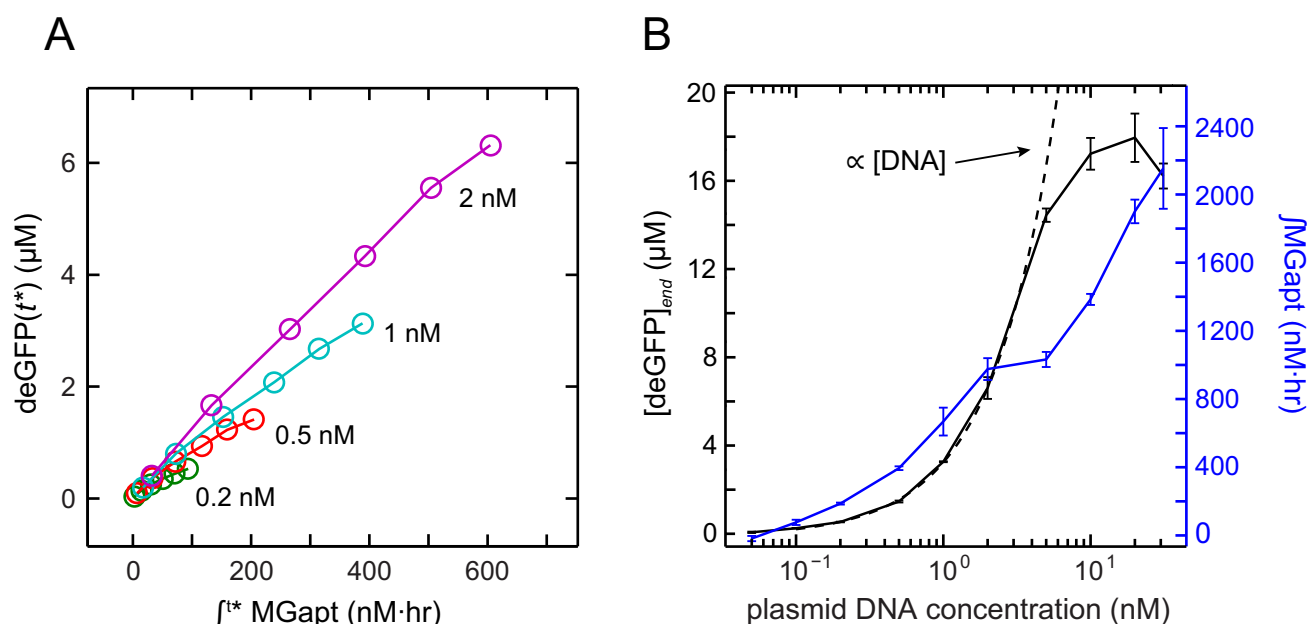


Figure 2: (A) deGFP versus integrated MGapt for the first six hours of expression for a range of DNA template concentrations. The relationship between them is linear as predicted by a simple model (Eq. 1). (B) Endpoint deGFP and integrated MGapt as a function of DNA template concentration. The endpoint deGFP level is proportional to the amount of template up to ~ 2 –5 nM.

DNA, $\int \text{MGapt}$ produced using Pr1 and Pr2 is 40% and 15% of the Pr value, respectively, and $[\text{deGFP}]_{\text{end}}$ is 11% and 0.4% of that produced by Pr. With 20 nM DNA, the percentages are different: $\int \text{MGapt}$ produced using Pr1 and Pr2 is 70% and 32% of Pr, respectively, and $[\text{deGFP}]_{\text{end}}$ is 30% and 2% of Pr. We note that at this higher concentration, the strong promoter is operating in the ‘saturation’ regime, while the weaker promoters are not.

The role of NTPs

The standard platform contains the natural NTPs essential for biocircuit operation, in concentrations of 1.5 mM ATP and GTP and 0.9 mM CTP and UTP [17]. Among their many cellular functions, ATP and GTP play a crucial role in translation, and all four NTPs are used in transcription as substrates in the synthesis of RNA. NTPs thus serve to couple a biocircuit’s transcription and translation layers together, with an impact that is not intuitively obvious but that can be significant (see, e.g., [18]). As a result, understanding precisely how changes in NTP concentration affect performance is of paramount importance.

We supplemented the system with an additional 1.25 mM of each NTP, an increase of $\sim 83\%$ ATP/GTP and $\sim 138\%$ CTP/UTP. In the linear regime, the extra NTPs have little effect on the shapes of the MGapt and deGFP profiles, save for an increase in $t_{\text{end},TL}$ to ~ 450 –500 minutes (Fig. S8). In the saturation regime however, the MGapt curves are broadened dramatically while the deGFP curves are more compressed at late times. The overall effect may be more easily seen on a plot of $[\text{deGFP}]_{\text{end}}$ versus $\int \text{MGapt}$ (Fig. 3). We find that the additional NTPs support a $\sim 30\%$ increase in $[\text{deGFP}]_{\text{end}}$ in the linear regime, a result that we primarily attribute to the increase in $t_{\text{end},TL}$. That is, the rate of production is relatively fixed but the productive period is extended. $\int \text{MGapt}$ also increases at low DNA concentrations. A more surprising result is seen at high DNA concentration, where $\int \text{MGapt}$ increases considerably but $[\text{deGFP}]_{\text{end}}$ is actually reduced by up to 20%. This suggests that NTPs do in fact help at the transcription level but that those excess transcripts are not translatable, and that perhaps the resources used to produce those transcripts

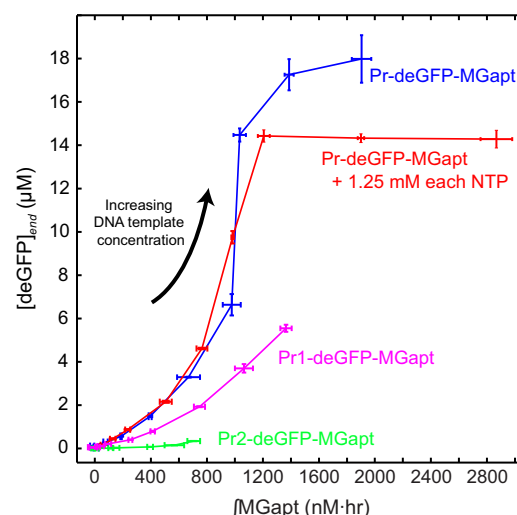


Figure 3: Endpoint deGFP versus integrated MGapt for three different promoters (Pr, Pr1, and Pr2) and with the cell-free breadboard supplemented with 1.25 mM of each of the four NTPs. DNA template concentrations are 0.02–20 nM.

may have been taken at the expense of reporter protein production.

Additional ‘housekeeping’ sigma factors

The association of a sigma factor (σ) with the catalytic core RNA polymerase (RNAP) is necessary for promoter recognition and transcription initiation in bacteria [19]. Thus, both σ and core RNAP are potential bottlenecks on transcription. In the cell-free breadboard, only the *E. coli* ‘housekeeping’ σ^{70} is present at appreciable concentrations [8]. To address the possibility that σ^{70} is in short supply and that it introduces an additional, NTP-independent limit on transcription capacity as a result, we supplemented the system with a plasmid carrying the σ^{70} gene under the control of the Pr promoter (Pr- σ^{70}) and assessed the system performance. Looking at MGapt kinetics at early times (Fig. 4), when resources that might otherwise be consumed in the production of σ^{70} are still plentiful, we see that 0.1–0.5 nM Pr- σ^{70} plasmid increases the level of MGapt relative to standard conditions. 1 nM Pr- σ^{70} only has a positive effect on MGapt levels with 10 nM Pr-deGFP-MGapt reporter DNA. Taken together these results suggest that additional σ^{70} does in fact help initiate more transcription events, although the effect is a mild one. We note that the Pr- σ^{70} kinetic traces deviate from the nominal curves at ~30–40 minutes, a time that allows for the accumulation of the additional σ^{70} protein. (Further discussion of the effect of additional σ^{70} can be found in the Supporting Information.)

Performance of a simple transcription-translation cascade

We also investigated the effect of adding an intermediate layer of transcription and translation on our reporters. The ‘cascade’ consists of constitutively-expressed T7 RNAP under the control of Pr, Pr1, or Pr2 and the deGFP-MGapt construct downstream of a T7-specific promoter (Fig. 5). T7 RNAP is convenient to use for this purpose since, unlike the native *E. coli* RNAP, it is a single-subunit RNAP that is easy to incorporate onto a single plasmid, and it does not compete with the core RNAP for sigma factors. This cascade circuit allows us to further determine if NTP consumption by transcription/

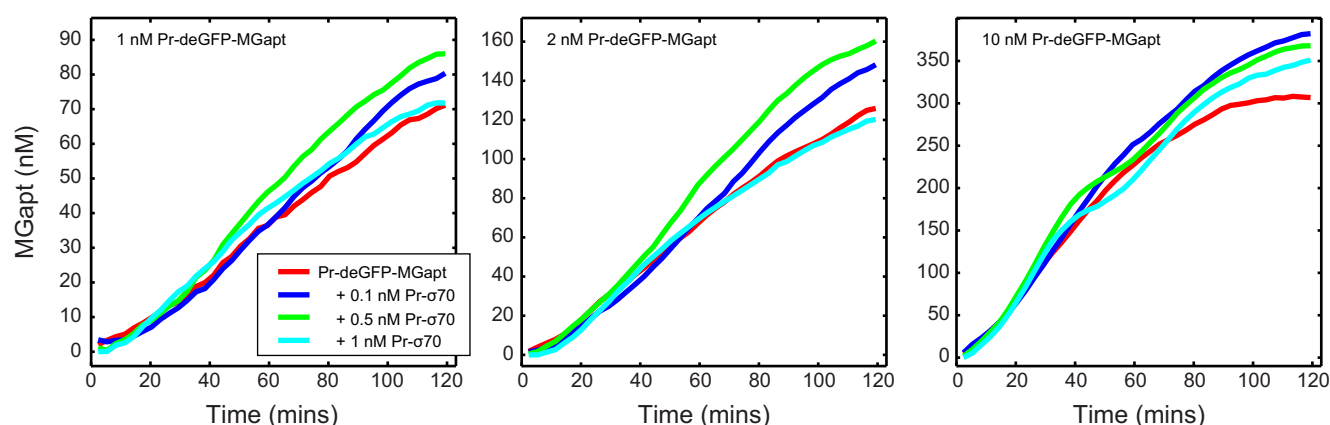


Figure 4: MGapt kinetics in the first 120 min of the experiment with different $\text{Pr-}\sigma^{70}$ and reporter DNA concentrations. Expression under standard conditions is shown in red. The addition of 0.1–0.5 nM $\text{Pr-}\sigma^{70}$ increases MGapt above the nominal case during this time. 1 nM $\text{Pr-}\sigma^{70}$ only has a positive effect with 10 nM reporter.

translation processes is a limiting factor, since the additional layer of transcription and translation would lead to a reduction in output relative to constitutive expression as it consumes more of these resources more quickly. Alternatively, if expression was limited (at least in part) by a reduction in the activity of the native RNAP, the introduction of T7 RNAP may extend the lifetime of the system.

There are substantial qualitative differences in T7 cascade expression as compared with a single-stage constitutive promoter. RNA increases rapidly and exhibits a long, slow decay (see, e.g., Fig. S9), and there is a ~30-60 minute delay in protein expression (see, e.g., Fig. S10). A higher reporter DNA concentration leads to a shorter delay and faster rise in expression, but the final deGFP concentration is often below the level achieved with a lower reporter concentration. This suggests a trade-off in cascade-driven protein production that may be the result of fuel consumption: if deGFP is produced more quickly, then the production appears to arrest sooner.

We find that the T7 cascade protein output is dictated by the concentration of the first-stage T7 RNAP plasmid and the identity of the promoter that drives T7 RNAP expression (Fig. 5). Weaker promoters (Pr1 and Pr2) controlling T7 RNAP expression lead to a wide range of deGFP levels with only small variations in the Pr1- and Pr2-T7 RNAP plasmid concentrations, and for any fixed concentration of the T7 RNAP plasmid, changes in reporter concentration (over an order of magnitude) do not affect deGFP output appreciably. When the strong Pr promoter is used, deGFP levels saturate at a level independent of the Pr-T7 RNAP concentration while MGapt levels vary substantially. The T7 cascade thus provides for independent tuning of RNA and protein outputs. Interestingly, we find regions of overlap where cascades with high concentrations of weaker first-stage promoters behave identically to low concentrations of stronger first-stage promoters. This equivalence was not present with the one-stage simple expression and may be due to the fact that in all versions of the cascade the promoters driving deGFP are identical.

In the simple expression case we found that adding NTPs to the system led to a considerable increase in transcription in the ‘saturation’ regime, but that the excess transcripts were not translated, and moreover that the resources used to produce those transcripts may have been taken at the expense of reporter protein production. We thus set out to see how the same addition of NTPs affects output of the T7 cascade with a strong first-stage promoter. As before, we supplemented the system with an additional 1.25 mM of each NTP. The resulting kinetics can be seen in Figs. S11 and S12, and compared with Figs. S9 and S10. Again we see a significant increase in the transcriptional activity; peaks are taller and broadened and the differences between different PT7-deGFP-MGapt concentrations are more pronounced. And while we do

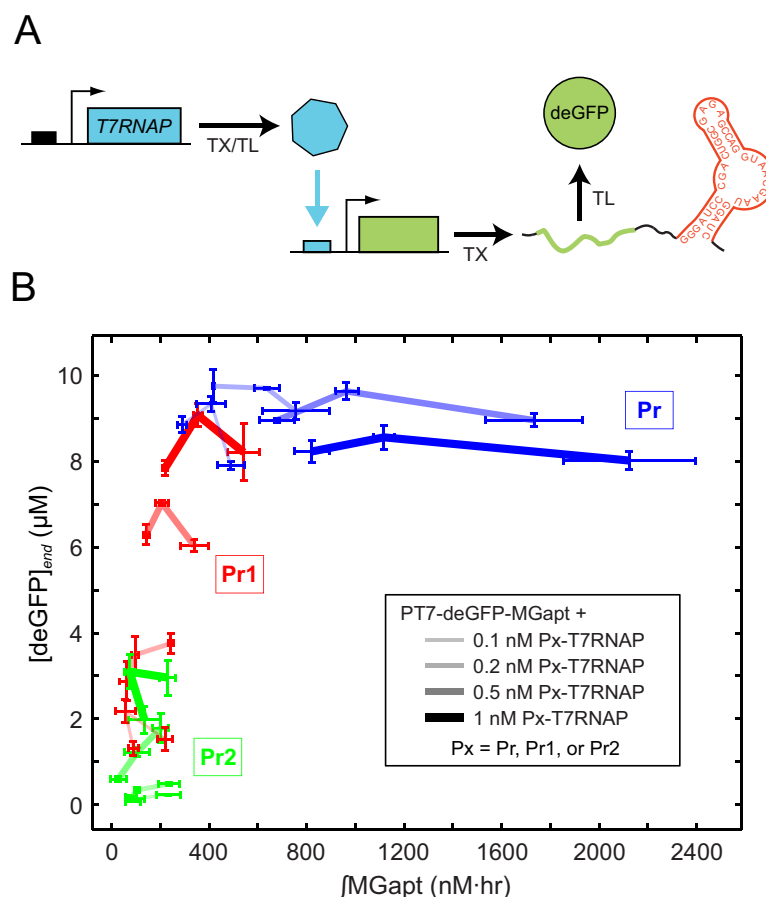


Figure 5: (A) The T7 cascade consists of constitutively-expressed T7 RNAP under the control of Pr, Pr1, or Pr2 and the deGFP-MGapt construct downstream of a T7-specific promoter. (B) Endpoint deGFP versus integrated MGapt for the T7 cascade with Pr-, Pr1-, or Pr2-T7 RNAP (0.1, 0.2, 0.5, and 1 nM) upstream of the PT7-deGFP-MGapt reporter (1, 2, and 10 nM).

not see a decrease in deGFP as we did with the Pr-deGFP-MGapt construct, there is little to be gained at the translational level by supplying excess NTPs.

Resource sharing and crosstalk between orthogonal genes

Recent work has highlighted indirect coupling between genes, or ‘crosstalk’, as a prominent side-effects of resource sharing in biocircuits [20–26]. Resources include those which are consumed during circuit operation (e.g., NTPs) as well as transcription/translation machinery that is present in limited amounts and that different parts of the circuit are forced to share. To clearly distinguish between crosstalk at the transcription stage (that may arise due to competition for RNAP or σ^{70}) and at the translation stage (arising from, e.g., a limited ribosome pool), we used a deCFP-MGapt reporter construct to assay system performance in the presence of two different loads: (1) the ‘native’ deGFP, containing the same UTR with strong RBS used throughout this work, and (2) deGFP with the RBS deleted from the UTR ($\Delta\text{RBS-deGFP}$). (We use the term ‘load’ to refer to components that consume some of the fixed transcriptional and translational capacity of the system, in analogy with electric loads that consume electric power.) Reporter and loads are all placed under the control of the same Pr promoter. The loads are orthogonal to the reporter in the sense that they have no direct regulatory interaction with it, as, e.g., activating or repressing transcription factors. With this particular setup, crosstalk at the transcription and translation

levels appears as changes in MGapt and deCFP fluorescence, respectively; with the Pr- Δ RBS-deGFP, any crosstalk must be strictly transcriptional as there is no RBS that can sequester ribosomes away from the production of deCFP.

We find that an increase in loading generally leads to a decrease in reporter expression, although it affects the transcription and translation levels differently (Fig. 6). For example, there is a similar ~ 250 nM-hr variation in \int MGapt as load increases for all reporter concentrations. At the translation level, however, the effect is highly dependent on load and reporter concentrations: the influence of the load on $[\text{deCFP}]_{\text{end}}$ is small at 1 nM reporter DNA but significant at 10 nM reporter. Thus, as the reporter DNA concentration increases, and the resources needed to produce reporter protein are more in demand, the translational crosstalk becomes much more pronounced. This also highlights the maximum translation capacity of the system that limits the total amount of protein that can be produced; as $[\text{deGFP}]_{\text{end}}$ goes up, $[\text{deCFP}]_{\text{end}}$ necessarily goes down. The top right corner of the $[\text{deGFP}]_{\text{end}}$ – $[\text{deCFP}]_{\text{end}}$ plot in Fig. 6 represents a translation performance regime that appears to be inaccessible.

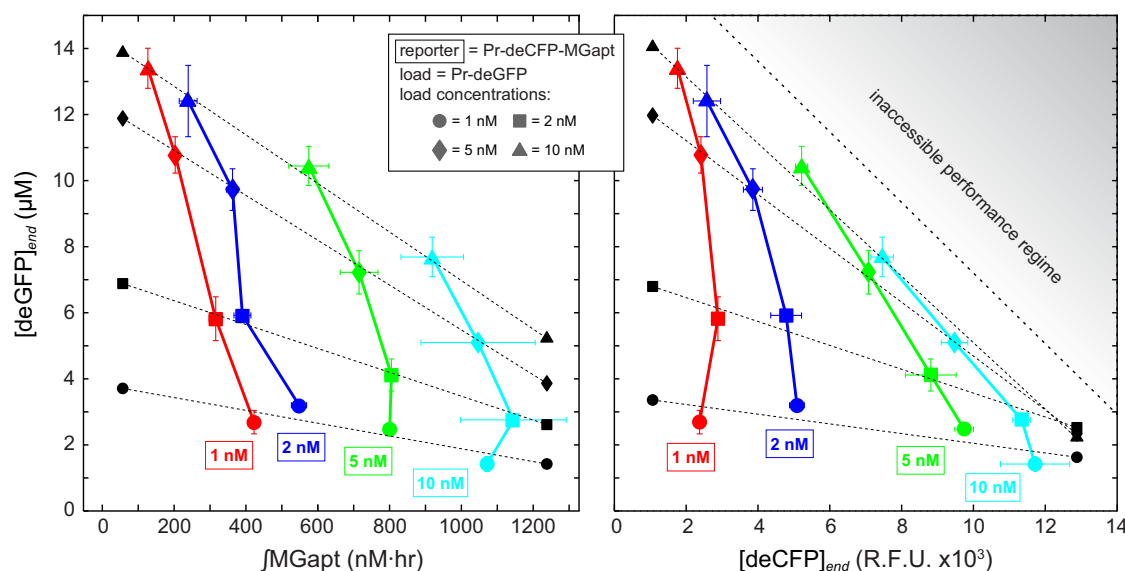


Figure 6: Endpoint deGFP versus integrated MGapt (left) and versus endpoint deCFP (right) following competitive expression of Pr-deCFP-MGapt and Pr-deGFP. The variation in $\int \text{MGapt}$ with increasing load is similar for all reporter concentrations, whereas at the translation level the crosstalk effect is highly dependent on load and reporter concentrations. There is a maximum translation capacity to the system that limits the total amount of protein that can be produced, as indicated by the inaccessible performance regime. Symbols indicate different concentrations of Pr-deGFP: \bullet = 1 nM, \blacksquare = 2 nM, \blacklozenge = 5 nM, and \blacktriangle = 10 nM.

The loading effects seen in Fig. 6 suggest that translation resources may be more limiting to system performance. To confirm this result, we compare the $\int \text{MGapt}$ – $[\text{deCFP}]_{\text{end}}$ relationships for Pr-deGFP and Pr- Δ RBS-deGFP (Fig. 7). When the RBS is present, in general we see that an increase in load leads to a decrease in $\int \text{MGapt}$ and $[\text{deCFP}]_{\text{end}}$ (Fig. 7, left). When the RBS is absent (Fig. 7, right), for the most part the load has no effect on performance, except for at high concentrations of both load and reporter, at which point we note a decrease in $[\text{deCFP}]_{\text{end}}$ and increase in $\int \text{MGapt}$.

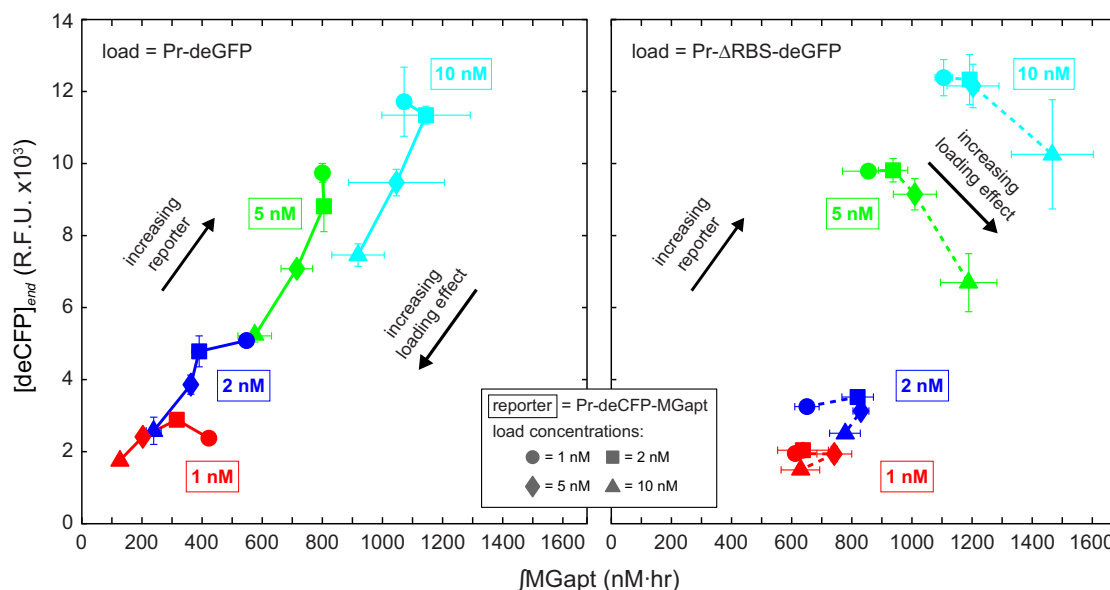


Figure 7: Effect of orthogonal Pr-deGFP (left) and Pr-ΔRBS-deGFP (right) loads on reporter expression. Increasing Pr-deGFP tends to decrease both $\int \text{MGapt}$ and $[\text{deCFP}]_{\text{end}}$. Without the RBS, only when load and reporter concentrations are high do we see a crosstalk effect: a decrease in $[\text{deCFP}]_{\text{end}}$ and increase in $\int \text{MGapt}$. Load concentrations are indicated as: ● = 1 nM, ■ = 2 nM, ◆ = 5 nM, and ▲ = 10 nM.

Discussion

Interest in simplified *in vitro* environments that approximate *in vivo* conditions is rooted in the desire to build and better understand biological circuits without the confounding factors that exist in live cells. Key to the success of these development and testing platforms is detailed and quantitative characterization. In this work we characterized a recently-developed, cell extract-based ‘breadboard’ which we then applied to the study of how biomolecular resources are used and shared in simple biocircuits. A novel reporter construct consisting of the malachite green RNA aptamer and a fluorescent protein allowed us to monitor transcription and translation simultaneously and in real-time. The use of the malachite green RNA aptamer may offer advantage over molecular beacons and binary probes [27, 28] in terms of wider dynamic range and faster response times. An analogous strategy connecting an RNA aptamer that mimics GFP [29] with fluorescent proteins spurred interest in concurrent measurement of transcription-translation activities *in vivo* [30, 31]. Recent studies have indicated that MGapt is also compatible with *in vivo* characterization of synthetic circuits [32], rendering this study relevant for *in vivo* studies as well as expanding the toolsets for real-time RNA monitoring with different spectral properties. Our results confirmed that transcriptional activity is a good predictor of translation-level behavior within a linear regime of DNA template concentrations for up to 6 hrs or more, beyond typical results for batch-mode cell-free reactions [14, 28]. On the other hand, the transcriptional and translational capacity of the system shows saturation dependent on different factors, adding to the consensus that there is significant value in the development and use of reliable transcription-translation reporters for concurrent mRNA and protein measurement.

In what follows we further discuss the connections between cell-free and *in vivo* results, and the implications of this work for more effective biocircuit prototyping.

Relevance for *in vivo*

While it can be expected that specific circuit behaviors will manifest themselves to different degrees in cell-free environments versus *in vivo*, nevertheless there is significant potential for cell-free work to contribute to understanding how circuits function in living systems. One example may be found in our ‘resource competition’ assays, through which we were able to quickly and clearly observe the translation machinery serving as a significant limiting resource. It has been suggested—by recent theoretical work [24] as well as by several other studies on ribosome utilization [25, 33–35]—that similar ribosome loading effects exist *in vivo*, despite the fact that live cells are able to produce additional translation machinery.

Other consequences of a limited ribosome pool found in the cell-free breadboard may also be found *in vivo*. In particular, it is known that translating ribosomes protect their template mRNAs from the action of endonucleases [36] and that ribosome spacing is a determinant of degradation rate [37]. Thus, if demands on a system are such that the available ribosome pool is insufficient to densely cover the number of transcripts, increased endonucleolytic activity would lead to an increase in the RNA degradation rate constant. Interestingly, a sharp increase in degradation rate constant is precisely what is seen in the MGapt expression profiles when the system transitions from the ‘linear’ to the ‘saturation’ regime (Fig. 1B).

Of course, ribosomes are not the only molecular resource that may be found in short supply and that can, as a result of their limited number, lead to crosstalk between unrelated circuits. Examples include the *E. coli* ClpXP protein degradation machinery [21] and transcription factors (TFs) with relatively large numbers of targets [38]. (Although the latter theoretical study dealt specifically with TF titration, the thermodynamic model may be generalizable to other ‘targeting’ biomolecules.) One particularly interesting class of candidate sources of crosstalk is the RNases. It has been suggested that competition for a relatively small number of RNases by a large number of RNA molecules can introduce unintended correlations [18], and evidence for this may be found in our results: the addition of the untranslated Δ RBS-deGFP load in amounts higher than or comparable to the reporter results in an increase in \int MGapt (Fig. 7). In this case, the load presents a large number of new targets for degradation enzymes, drawing them away from the RNA reporter and thus indirectly leading to the increase in \int MGapt. We are currently unaware of *in vivo* results demonstrating crosstalk-via-RNases; however, given the ribosome loading effects seen in both cell-free and *in vivo* systems, it is an intriguing possibility worthy of exploration, with particular relevance for RNA-based synthetic regulatory circuits [39–41].

And there are still other examples of how the cell-free breadboard may be used to predict or confirm various effects that arise in cells due to resource limits. In a recent modeling study it was suggested that different combinations of promoter and RBS strengths can result in comparable protein output with different loads on the cellular expression machinery, and that codon usage can introduce a bottleneck that impacts the expression of other genes [42]. The degree of precise control that exists in the cell-free breadboard—for example, control over DNA concentration and known induction levels without an intervening cell membrane—makes it an ideal platform for investigating this and other related questions.

On biocircuit prototyping

Despite recent developments in standardized part libraries and rapid assembly tools (e.g., [43, 44]), synthetic biology still lacks the accepted prototyping platforms and protocols common to other engineering disciplines. For the purposes of prototyping, one particular advantage of our cell-free breadboard is the rapid testing cycle it permits: save for the initial cloning, transformation, and plasmid preparation, none of the individual assays performed in this work required the many hours of cell treatment typically needed for *in vivo* studies. With plasmids in hand, the time from cell-free experiment setup to first results is a matter of minutes.

Problems associated with limits on the cell-free breadboard system capacity may be mitigated when operating in regimes that yield predictable response; the ‘linear’ regime, for example, where the protein production rate is constant until a well-defined end time and the amount of protein is proportional to

template DNA concentration. The ‘linear’ regime boundaries can change with promoter strength and NTP concentration, as shown in Fig. 8. But even when the strongest promoter Pr is used, we find that we can achieve ~ 6 hours of predictable performance, with measurable FP signal over a wide range of DNA template concentrations. We advocate using the ‘linear’ regime for cell-free circuit testing or other applications that require linear response. The ‘saturation’ regime may be used when maximum yield is desired but the linearity of the DNA–protein relationship is not essential.

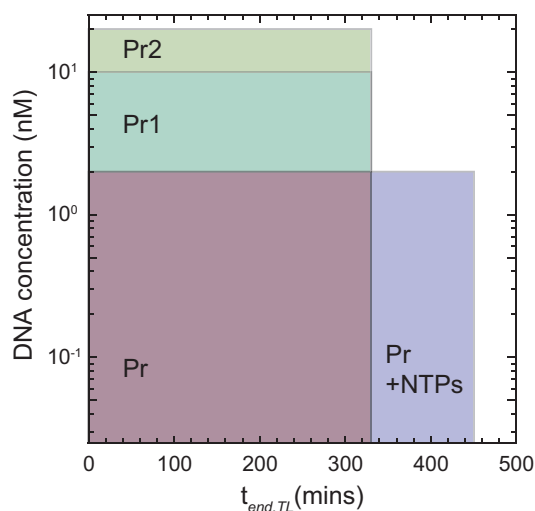


Figure 8: DNA concentration and protein production time boundaries of the ‘linear’ regime.

And there are a number of ways in which limits on the capacity of the cell-free breadboard may be raised. The functional lifetime of the system, which in bulk operation is limited by unidentified mechanisms reducing the activity of the transcription/translation machinery, may be increased using dialysis membranes and vesicles, up to 16 and 100 hours, respectively [8,45]. Reaction times may be further extended with the use of microfluidics or other continuous-flow devices, as demonstrated with other cell-free environments [46, 47]. Also, the addition of purified proteins such as T7 RNAP or σ^{70} could potentially support an increase in capacity at no additional cost to the system; in related work it has been shown that purified GamS protein can be added to prevent degradation of linear DNA [9]. Ideally, a combination of strategies should be employed to take maximum advantage of the cell-free breadboard. The ease with which these strategies can be employed, along with the relative simplicity of the system and the control that it offers, makes it a promising platform for synthetic biocircuit prototyping.

Materials and Methods

Cell-free system and reactions

The breadboard environment consists of a crude cytoplasmic extract from *E. coli* containing soluble proteins, including the entire endogenous transcription-translation machinery and mRNA and protein degradation enzymes [7,8]. Detailed instructions for extract preparation can be found in [17]. To avoid variation between different extract preparations we used the same batch of extract for all experiments. Reactions took place in 10 μ l volumes at 29°C. No significant toxicity was observed for typical deGFP expression experiments when up to 20 μ M malachite green (MG) dye was included in the reaction; the MG dye concentration was thus fixed at 10 μ M for all experiments.

Reporters

Real-time fluorescence monitoring of mRNA dynamics was performed using the malachite green aptamer (MGapt) [12] incorporated in the 3' UTR of the fluorescent protein reporter genes, 15 bases downstream of the stop codons. This location of MGapt insertion was chosen after a number of other possible locations were tested and found to give less accurate measures of RNA dynamics. For example, incorporation of MGapt within the 5' UTR upstream of the RBS led to decreased MGapt fluorescence signal, a result that may be due to the preference of 5' end degradation by the dominant endonuclease in *E. coli*, RNase E [48]. This is consistent with a recent study on the Spinach fluorescent RNA aptamer [30] in which it was reported that incorporation of the aptamer in the 3' UTR region led to stronger fluorescence than in the 5' UTR. It was also found that a 6-base spacing between the stop codon of deGFP and MGapt affected the protein expression level to some extent, but a 10-base and 15-base spacing showed equivalent MGapt fluorescence signal levels without affecting protein expression. The fluorescent proteins deGFP and deCFP were previously designed to be more translatable in the cell-free system [7]. The UTR controlling translation of deGFP (eGFP- Δ_{6-229}) and deCFP contained the T7 gene 10 leader sequence for highly efficient translation initiation [7]. All transcription units included the T500 transcriptional terminator except for PT7-deGFP-MGapt which contained T7 terminator.

Fluorescence measurements were made in triplicate in a Biotek plate reader at 3 minute intervals using excitation/emission wavelengths set at 610/650 nm (MGapt), 485/525 nm (deGFP), and 433/475 nm (deCFP). Error bars in figures showing fluorescence or integrated fluorescence indicate standard error over replicates.

Plasmids and Bacterial strains

Plasmids was created using standard cloning methods. The plasmid pBEST-Luc (Promega) was used as a template for all constructs except for the PT7-deGFP-MGapt construct which was derived from the plasmid pIVEX2.3d (Roche). The same antibiotic resistance gene was used with each plasmid to ensure that any burden on the system due to the expression of these 'background' proteins was the same for each construct. All plasmids used are listed in Table S1. Plasmid DNAs used in cell-free experiments were prepared using Qiagen Plasmid Midi prep kits. *E. coli* strains KL740 (which contains lambda repressor to control for Pr promoter) or JM109 were used. LB media with 100 μ g/mL carbenicillin was used to culture cells.

Promoters Pr1 and Pr2 were each modified from Pr with a single base mutation in the -35 and -10 region, respectively. The sequences, with mutations highlighted by \square , are

Pr: TGAGCTAACACCGTGCGTGTGACAATTTTACCTCTGGCGGTGATAATGGTTGCA

Pr1: TGAGCTAACACCGTGCGTGT \square GACAATTTTACCTCTGGCGGTGATAATGGTTGCA

Pr2: TGAGCTAACACCGTGCGTGTGACAATTTTACCTCTGGCGGTG \square TAATGGTTGCA

Preparation of pure mRNA and qRT-PCR

RNA was transcribed using a linear template PCR-amplified from pIVEX2.3d PT7-deGFP-MGapt including T7 promoter and T7 terminator region. The transcription reaction was prepared as a total volume of 100 μ L with 0.1 μ M linear DNA template, 20% (v/v) T7 RNA polymerase (Cellscript), 7.5 mM each NTP (Epicentre), 24 mM MgCl₂ (Sigma), 10% (v/v) 10 \times transcription buffer, and 1% (v/v) thermostable inorganic pyrophosphatase (New England Biolabs). After an overnight incubation at 37°C, the reaction mixture was run on 1% agarose gel, RNA bands that correspond to full-length transcript were excised and eluted from gel by the Freeze-N-Squeeze column (Biorad) and resuspended in water. Concentrations of purified RNA were determined spectrophotometrically using Nanodrop.

For qRT-PCR, 1 μ L samples were taken at different time points from a tube containing reaction mixture at 29°C and diluted 50-fold in water. These samples were stored at -80°C until used. Afterward the samples

were further diluted to a final dilution of 1:5000. Two μL of samples were analyzed in 50 μL reactions of the Power SYBR Green RNA-to-CT 1-Step kit (Life Technologies) in the MX3005 real-time PCR machine (Agilent Technologies). Primers amplified a region of the deGFP gene closer to its 3' end (424-597 nt) and were used at 0.3 μM concentrations. Concentrations of deGFP-MGapt RNA in the sample were determined from a standard curve of dilutions of purified mRNA in a range from 0.6 to 60 pM mRNA per PCR reaction.

Acknowledgments

The authors would like to thank Eduardo Sontag and members of the Murray Group for useful discussions, and S. C. Livingston and P. Rovo for helpful comments on the manuscript. This research is funded in part by the Gordon and Betty Moore Foundation through Grant GBMF2809 to the Caltech Programmable Molecular Technology Initiative, and by the Defense Advanced Research Projects Agency (DARPA/MTO) Living Foundries program, contract number HR0011-12-C-0065. Z.A.T. was partially supported by grants TAMOP-4.2.1-B-11/2/KMR-2011-0002, TAMOP-4.2.2./B-10/1-2010-0014 and OTKA NF 104706.

The views and conclusions contained in this document are those of the authors and should not be interpreted as representing official policies, either expressly or implied, of the Defense Advanced Research Projects Agency or the U.S. Government.

References

- [1] Allen A Cheng and Timothy K Lu. Synthetic biology: an emerging engineering discipline. *Annu Rev Biomed Eng*, 14:155–178, 2012.
- [2] Stefano Cardinale and Adam P Arkin. Contextualizing context for synthetic biology - identifying causes of failure of synthetic biological systems. *Biotechnol J*, 7(7):856–866, July 2012.
- [3] Caleb J Bashor and James J Collins. Insulating gene circuits from context by RNA processing. *Nat Biotechnol*, 30(11):1061–1062, November 2012.
- [4] Stefano Cardinale, Marcin Pawel Joachimiak, and Adam P Arkin. Effects of Genetic Variation on the *E. coli* Host-Circuit Interface. *Cell Reports*, 4(2):231–237, July 2013.
- [5] P Marguet, Y Tanouchi, E Spitz, C Smith, and L You. Oscillations by minimal bacterial suicide circuits reveal hidden facets of host-circuit physiology. *PLoS ONE*, 5(7):e11909, 2010.
- [6] Cheemeng Tan, Philippe Marguet, and Lingchong You. Emergent bistability by a growth-modulating positive feedback circuit. *Nat Chem Biol*, 5(11):842–848, November 2009.
- [7] Jonghyeon Shin and Vincent Noireaux. Efficient cell-free expression with the endogenous *E. Coli* RNA polymerase and sigma factor 70. *J Biol Eng*, 4:8, 2010.
- [8] Jonghyeon Shin and Vincent Noireaux. An *E. coli* Cell-Free Expression Toolbox: Application to Synthetic Gene Circuits and Artificial Cells. *ACS Synth Biol*, 1(1):29–41, January 2012.
- [9] Zachary Z Sun, Enoch Yeung, Clarmyra A Hayes, Vincent Noireaux, and Richard M Murray. Linear DNA for rapid prototyping of synthetic biological circuits in an *Escherichia coli* based TX-TL cell-free system. *ACS Synth Biol (in press)*, 2013.
- [10] C Eric Hodgman and Michael C Jewett. Cell-free synthetic biology: thinking outside the cell. *Metabolic Engineering*, 14(3):261–269, May 2012.
- [11] James Chappell, Kirsten Jensen, and Paul S Freemont. Validation of an entirely in vitro approach for rapid prototyping of DNA regulatory elements for synthetic biology. *Nucleic Acids Res*, 41(5):3471–3481, March 2013.
- [12] Dilara Grate and Charles Wilson. Laser-mediated, site-specific inactivation of RNA transcripts. *Proc Natl Acad Sci USA*, 96:6131–6136, 1999.
- [13] Eyal Karzbrun, Jonghyeon Shin, Roy Bar-Ziv, and Vincent Noireaux. Coarse-grained dynamics of protein synthesis in a cell-free system. *Phys Rev Lett*, 106(4):048104, January 2011.
- [14] Tobias Stögbauer, Lukas Windhager, Ralf Zimmer, and Joachim O Rädler. Experiment and mathematical modeling of gene expression dynamics in a cell-free system. *Integr Biol*, 4(5):494–501, May 2012.
- [15] Michael C Jewett and James R Swartz. Substrate replenishment extends protein synthesis with an in vitro translation system designed to mimic the cytoplasm. *Biotechnol Bioeng*, 87(4):465–472, August 2004.
- [16] D M Kim and J R Swartz. Prolonging cell-free protein synthesis with a novel ATP regeneration system. *Biotechnol Bioeng*, 66(3):180–188, 1999.

- [17] Zachary Z Sun, Clarmyra A Hayes, Jonghyeon Shin, Filippo Caschera, Richard M Murray, and Vincent Noireaux. Protocols for Implementing an Escherichia coli Based TX-TL Cell-Free Expression System for Synthetic Biology. *J Vis Exp*, 79:e50762, 2013.
- [18] Enoch Yeung, Jongmin Kim, Ye Yuan, Jorge Goncalves, and Richard M Murray. Quantifying crosstalk in biochemical systems. In *51st IEEE Conference on Decision and Control (CDC)*, pages 5528–5535, Maui, HI, December 2012.
- [19] Sofia Österberg, Teresa del Peso-Santos, and Victoria Shingler. Regulation of alternative sigma factor use. *Annu Rev Microbiol*, 65:37–55, 2011.
- [20] Dan Siegal-Gaskins, Vincent Noireaux, and Richard M Murray. Biomolecular resource utilization in elementary cell-free gene circuits. In *American Control Conference (ACC), 2013*, pages 1531–1536, 2013.
- [21] Natalie A Cookson, William H Mather, Tal Danino, Octavio Mondragón-Palomino, Ruth J Williams, Lev S Tsimring, and Jeff Hasty. Queueing up for enzymatic processing: correlated signaling through coupled degradation. *Mol Syst Biol*, 7:561, 2011.
- [22] Matthew Scott, Carl W Gunderson, Eduard M Mateescu, Zhongge Zhang, and Terence Hwa. Interdependence of cell growth and gene expression: origins and consequences. *Science*, 330(6007):1099–1102, November 2010.
- [23] William H Mather, Natalie A Cookson, Jeff Hasty, Lev S tsimring, and Ruth J Williams. Correlation resonance generated by coupled enzymatic processing. *Biophys J*, 99(10):3172–3181, November 2010.
- [24] William H Mather, J Hasty, L S Tsimring, and R J Williams. Translational Cross Talk in Gene Networks. *Biophys J*, 2013.
- [25] Dominique Chu, David J Barnes, and Tobias von der Haar. The role of tRNA and ribosome competition in coupling the expression of different mRNAs in *Saccharomyces cerevisiae*. *Nucleic Acids Res*, 39(15):6705–6714, August 2011.
- [26] Y Rondelez. Competition for Catalytic Resources Alters Biological Network Dynamics. *Phys Rev Lett*, 108(1):018102, 2012.
- [27] Salvatore A.E. Marras, Sanjay Tyagi, and Fred Russell Kramer. Real-time assays with molecular beacons and other fluorescent nucleic acid hybridization probes. *Clinica Chimica Acta*, 363:48–60, 2006.
- [28] Henrike Niederholtmeyer, Ling Xu, and Sebastian J. Maerkl. Real-time mRNA measurement during an in vitro transcription and translation reaction using binary probes. *ACS Synth Biol*, 2:411–417, 2013.
- [29] Jeremy S. Paige, Karen Wu, and Samie R. Jaffrey. RNA mimics of green fluorescent protein. *Science*, 333:642–646, 2011.
- [30] Georgios Pothoulakis, Francesca Ceroni, Benjamin Reeve, and Tom Ellis. The Spinach RNA Aptamer as a Characterization Tool for Synthetic Biology. *ACS Synth Biol*, September 2013.
- [31] Pauline van Nies, Zohreh Nourian, Maurits Kok, Roeland van Wijk, Jonne Moeskops, Ilja Westerlaken, Jos M Poolman, Rienk Eelkema, Jan H van Esch, Yutetsu Kuruma, Takuya Ueda, and Christophe Danelon. Unbiased Tracking of the Progression of mRNA and Protein Synthesis in Bulk and in Liposome-Confined Reactions. *Chembiochem*, 14(15):1963–1966, October 2013.

- [32] Andrew Ng, Enoch Yeung, and Richard M. Murray. Understanding the effects of compositional context on biocircuit performance. *Submitted*, 2013.
- [33] J Vind, M A Sørensen, M D Rasmussen, and S Pedersen. Synthesis of proteins in Escherichia coli is limited by the concentration of free ribosomes. Expression from reporter genes does not always reflect functional mRNA levels. *J Mol Biol*, 231(3):678–688, June 1993.
- [34] Namiko Mitarai, Kim Sneppen, and Steen Pedersen. Ribosome collisions and translation efficiency: Optimization by codon usage and mRNA destabilization. *Journal of Molecular Biology*, 382:236–245, 2008.
- [35] Michael A. Sørensen and Steen Pedersen. Absolute in vivo translation rates of individual codons in escherichia coli: the two glutamic acid codons GAA and GAG are translated with a threefold difference in rate. *Journal of Molecular Biology*, 222:265–280, 1991.
- [36] Atilio Deana and Joel G Belasco. Lost in translation: the influence of ribosomes on bacterial mRNA decay. *Genes Dev*, 19(21):2526–2533, November 2005.
- [37] Margit Pedersen, Søren Nissen, Namiko Mitarai, Sine Lo Svenningsen, Kim Sneppen, and Steen Pedersen. The functional half-life of an mRNA depends on the ribosome spacing in an early coding region. *J Mol Biol*, 407(1):35–44, March 2011.
- [38] Mattias Rydenfelt, Robert Sidney Cox, III, Hernan Garcia, and Rob Phillips. The transcription factor titration effect: statistical mechanical model of coupled transcription from multiple promoters. *Phys Rev E (in press)*, 2013.
- [39] Farren J Isaacs, Daniel J Dwyer, Chunming Ding, Dmitri D Pervouchine, Charles R Cantor, and James J Collins. Engineered riboregulators enable post-transcriptional control of gene expression. *Nat Biotechnol*, 22:841–847, 2004.
- [40] Julius B. Lucks, Lei Qi, Vivek K. Mutalik, Denise Wang, and Adam P. Arkin. Versatile RNA-sensing transcriptional regulators for engineering genetic networks. *Proc Natl Acad Sci USA*, 108:8617–8622, 2011.
- [41] Guillermo Rodrigo, Thomas E. Landrain, and Alfonso Jaramillo. De novo automated design of small rna circuits for engineering synthetic riboregulation in living cells. *Proc Natl Acad Sci USA*, 109:15271–15276, 2012.
- [42] Rhys Algar, Tom Ellis, and Guy-Bart Stan. Modelling the burden caused by gene expression: an in silico investigation into the interactions between synthetic gene circuits and their chassis cell. *arXiv*, September 2013.
- [43] Kevin D Litcofsky, Raffi B Afeyan, Russell J Krom, Ahmad S Khalil, and James J Collins. Iterative plug-and-play methodology for constructing and modifying synthetic gene networks. *Nat Meth*, 9(11):1077–1080, November 2012.
- [44] Sean C Sleight and Herbert M Sauro. Randomized BioBrick Assembly: A Novel DNA Assembly Method for Randomizing and Optimizing Genetic Circuits and Metabolic Pathways. *ACS Synth Biol*, July 2013.
- [45] Vincent Noireaux and Albert Libchaber. A vesicle bioreactor as a step toward an artificial cell assembly. *Proc Natl Acad Sci USA*, 101(51):17669–17674, December 2004.
- [46] Qian Mei, Ruba Khnouf, Andrew Simon, and Z Hugh Fan. Protein synthesis in a device with nanoporous membranes and microchannels. *Lab Chip*, 10(19):2541–2545, October 2010.

- [47] Henrike Niederholtmeyer, Viktoria Stepanova, and Sebastian J Maerkl. Implementation of cell-free biological networks at steady state. *Proc Natl Acad Sci USA*, 110(40):15985–15990, October 2013.
- [48] George A Mackie. RNase E: at the interface of bacterial RNA processing and decay. *Nat Rev Microbiol*, 11(1):45–57, January 2013.

Supporting Information

Relationship between integrated MGapt and deGFP concentration

Throughout this work we have used the amount of MGapt integrated over the course of the experiment ($\int_{t=0}^{t_{end}} \text{MGapt}(t') dt' = \int \text{MGapt}$) and the concentration of deGFP at the end of the experiment ($\text{deGFP}(t_{end}) = [\text{deGFP}]_{end}$) as measures of transcription- and translation-level performance. While the proportionality between $\text{deGFP}(t^*)$ and $\int^{t^*} \text{MGapt}$ would hold true for all times t^* in the absence of protein degradation and under the naive assumptions of unlimited resources and conditions unchanging with time, the actual relationship between deGFP and MGapt is more complicated, a result of resource limits and changing environmental conditions. In Fig. S1 we show $\text{deGFP}(t^*)$ versus $\int^{t^*} \text{MGapt}$, for $t^* = 1, 2, \dots, 14$ hrs and for a range of Pr-deGFP-MGapt concentrations. As was also seen in Fig. 1B, there are two operational regimes separated by a concentration threshold. Below 5 nM plasmid DNA—the previously-described ‘linear’ regime in which $[\text{deGFP}]_{end}$ scales linearly with the DNA template concentration— $\int^{t^*} \text{MGapt}$ is proportional to $\text{deGFP}(t^*)$ until protein synthesis stops at $t^* \approx 350$ minutes (even though transcriptional activity continues). It is only during this period of time that transcriptional activity is a good predictor of what happens at the level of translation. Above the threshold concentration, in the ‘saturation’ regime where $[\text{deGFP}]_{end}$ is sublinear with respect to the amount of DNA template, protein production continues for longer and the $\int^{t^*} \text{MGapt}$ plateau is shorter than in the ‘linear’ regime. Precisely why protein production is sharply cut-off at low template concentrations and extended (albeit at a reduced rate) at high template concentrations, is unknown. But for circuit design and testing applications, these empirical results are worth noting: one can expect linear response at the translation level up to a fixed time only when operating in the ‘linear’ regime, and while protein production can continue for longer times when template concentration lies in the ‘saturation’ regime, the response is sublinear.

The effect of additional Pr- σ^{70} on $\int \text{MGapt}$ and $[\text{deGFP}]_{end}$

The overall effect of additional Pr- σ^{70} is nonintuitive and dependent on both the Pr- σ^{70} and reporter concentrations. $[\text{deGFP}]_{end}$ versus $\int \text{MGapt}$ for the baseline construct with various concentrations Pr- σ^{70} is shown in Fig. S2. Compared with standard conditions, we see that low levels of Pr- σ^{70} (0.1–0.5 nM) lead to increased $\int \text{MGapt}$ /decreased $[\text{deGFP}]_{end}$ with 10 nM reporter, decreased $\int \text{MGapt}$ /increased $[\text{deGFP}]_{end}$ with 2 nM reporter, and an increase in $[\text{deGFP}]_{end}$ with no change in $\int \text{MGapt}$ with 1 nM reporter. The system shows signs of being overburdened by 1 nM Pr- σ^{70} DNA, with relative decreases in both $\int \text{MGapt}$ and $[\text{deGFP}]_{end}$ for all reporter concentrations. This would suggest that the substantial amount of additional DNA may be sequestering away resources required for reporter production, even if in this case the DNA codes for proteins that are ostensibly helpful.

Alternative performance metrics

For the purposes of characterization of a particular biocircuit testing environment, *in vitro* or *in vivo*, there are any number of performance metrics that may be used. We have chosen to use integrated mRNA and final protein concentration since they intuitively represent the total transcriptional and translational capacity of a system. Other metrics, such as the mRNA and protein production rates and end times, are complementary to those used in this work and may in fact be more informative depending on the specific circuit or system requirement.

In Figs. S13 and S14 we show the maximum deGFP and MGapt production rates as a function of reporter concentration under different conditions. Using these measures, stark differences between simple one-stage gene expression and expression from the two-stage T7 cascade can be seen; for example, at low reporter concentrations, the maximum production rate of deGFP in the cascade is considerably larger than the one-stage rate, even when the strongest promoter is used. The cascade deGFP rates are also relatively

flat with respect to reporter concentration. There is also a clear effect of NTPs on peak rates when a cascade is used versus simple expression. In the former case, additional NTPs provide for a significant increase in the maximum protein and mRNA production rates, whereas NTPs have little to no effect on maximum production rates for the Pr-deGFP-MGapt construct.

The deGFP production end time $t_{end,TL}$, defined as the time at which the deGFP level reaches 95% of its final value, is shown for all conditions in Fig. S15. $t_{end,TL}$ is between 330 and 350 minutes for simple expression in the ‘linear’ regime, but as high as ~ 580 minutes in some of the conditions and concentrations tested. The end time is a particularly good measure of system capacity when extended performance is required.

Supplementary Figures

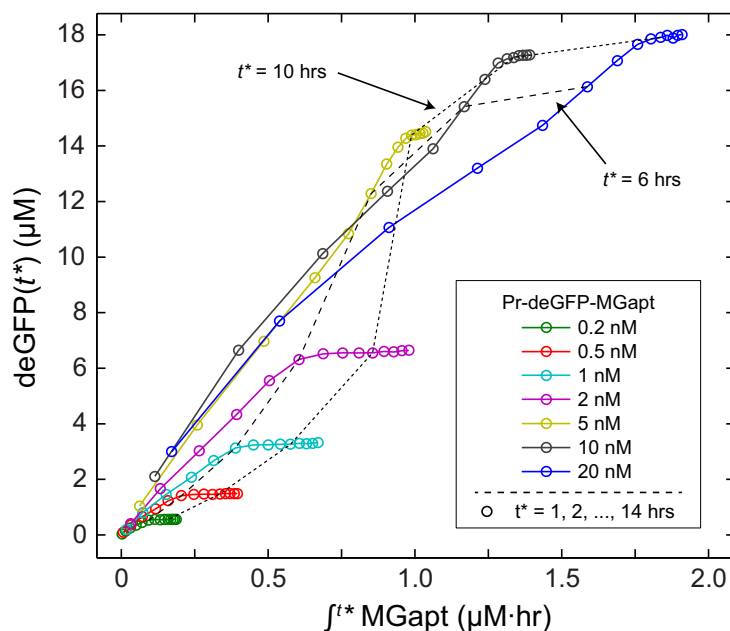


Figure S1: deGFP at various times t^* (deGFP(t^*)) versus MGapt level integrated from time $t = 0$ to $t = t^*$ ($\int t^* \text{MGapt}$) for a range of Pr-deGFP-MGapt concentrations, with $t^* = 1, 2, \dots, 14$ hrs indicated with \circ . Below the ‘linear’-‘saturation’ regime transition concentration, $\int t^* \text{MGapt}$ appears proportional to deGFP(t^*) until protein synthesis stops at $t^* \approx 350$ minutes. Above the transition concentration, protein production stops later in the experiment and the $\int t^* \text{MGapt}$ plateau is relatively short. Dashed lines showing $t^* = 6$ hrs and $t^* = 10$ hrs are shown for reference.

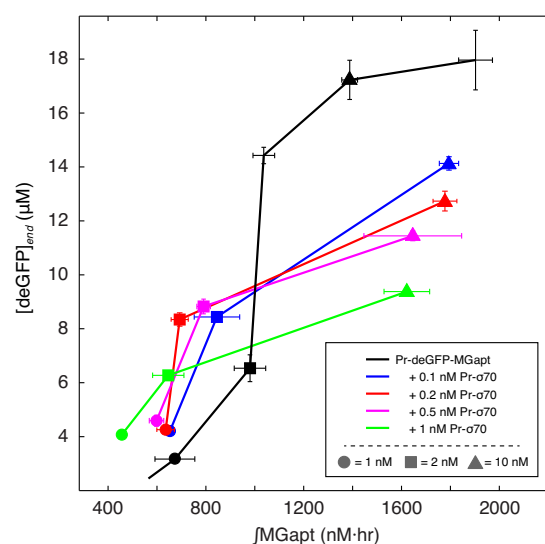


Figure S2: Endpoint deGFP versus integrated MGapt for Pr-deGFP-MGapt when the cell-free breadboard is supplemented with different concentrations of Pr- σ^{70} (\bullet = 1 nM, \blacksquare = 2 nM, \blacktriangle = 10 nM). Relative to performance under standard conditions, low levels of Pr- σ^{70} (0.1–0.5 nM) lead to increased \int MGapt/decreased $[\text{deGFP}]_{\text{end}}$ with 10 nM reporter, decreased \int MGapt/increased $[\text{deGFP}]_{\text{end}}$ with 2 nM reporter, and an increase in $[\text{deGFP}]_{\text{end}}$ with no change in \int MGapt with 1 nM reporter. The system shows signs of being overburdened by 1 nM Pr- σ^{70} DNA, with relative decreases in both \int MGapt and $[\text{deGFP}]_{\text{end}}$ for all reporter concentrations.

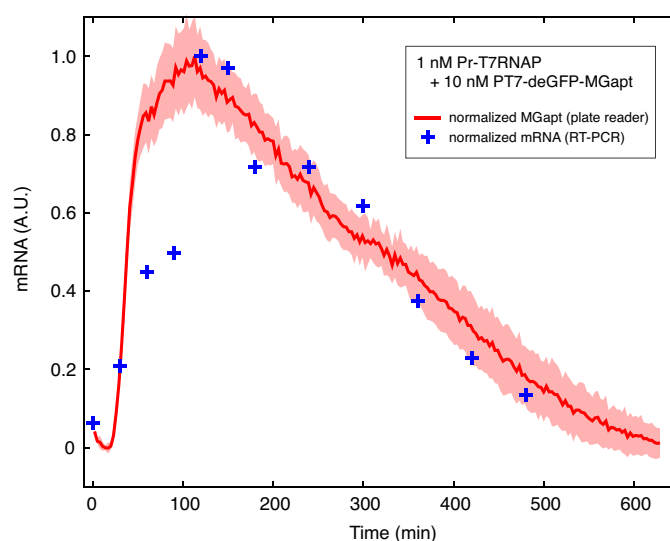


Figure S3: Comparison of normalized real-time PCR measurements and MGapt signal for T7 cascade circuit, with 1 nM Pr-T7 RNAP and 10 nM PT7-deGFP-MGapt. Shaded region indicates standard error over replicates.

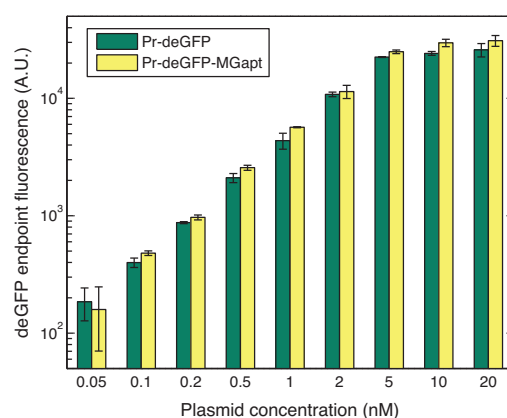


Figure S4: Comparison of total deGFP fluorescence produced by Pr-deGFP and Pr-deGFP-MGapt constructs. The incorporation of MGapt in the 3' UTR downstream of deGFP leads to only a slight increase in the amount of protein produced relative to deGFP alone, a result we attribute to an increase in the stability of the fusion transcript conferred by the MGapt.

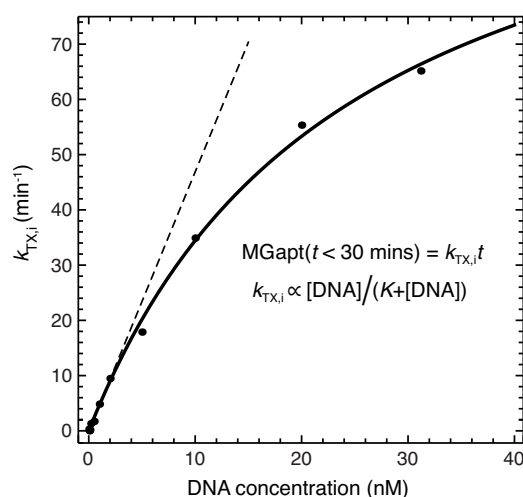


Figure S5: Rates of MGapt production in the first 30 minutes of expression follow a Michaelis-Menten form, saturating at high DNA concentrations. The Michaelis constant K is ~ 24 nM.

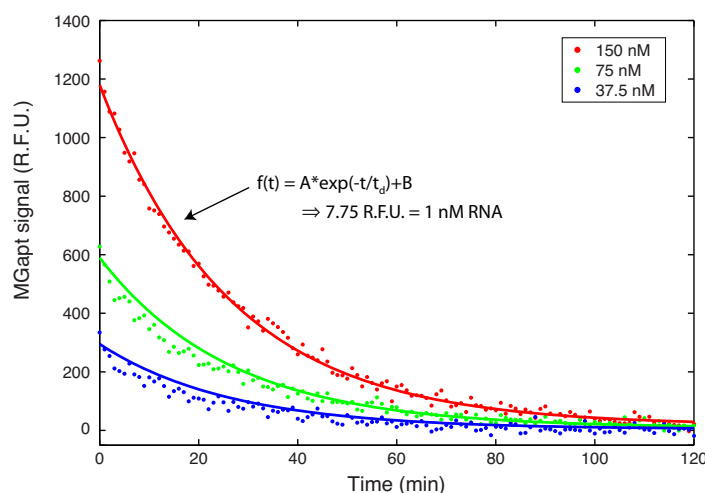


Figure S6: Decay curves for three different initial concentrations of purified deGFP-MGapt RNA.

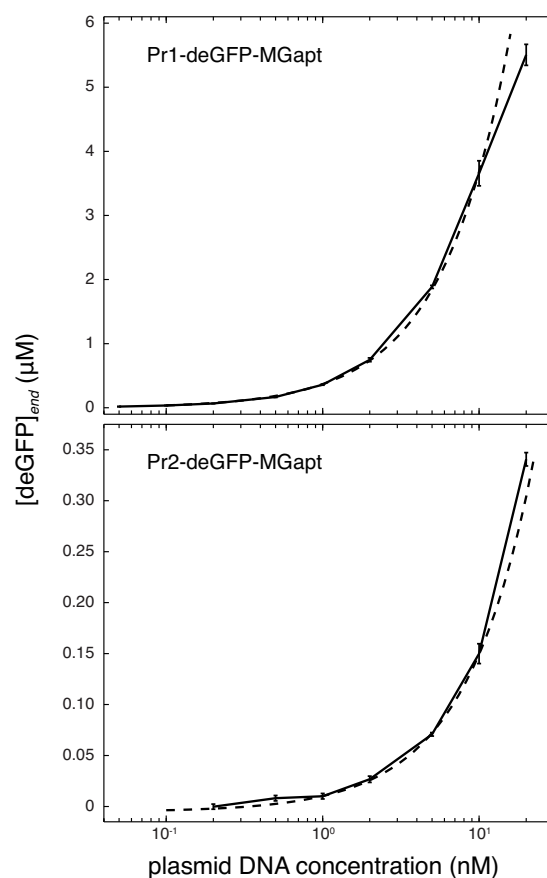


Figure S7: For deGFP-MGapt driven by weak promoters Pr1 and Pr2, the linear regime extends up to ~10 nM and ~20 nM, respectively. Dashed line shows a linear fit to the data.

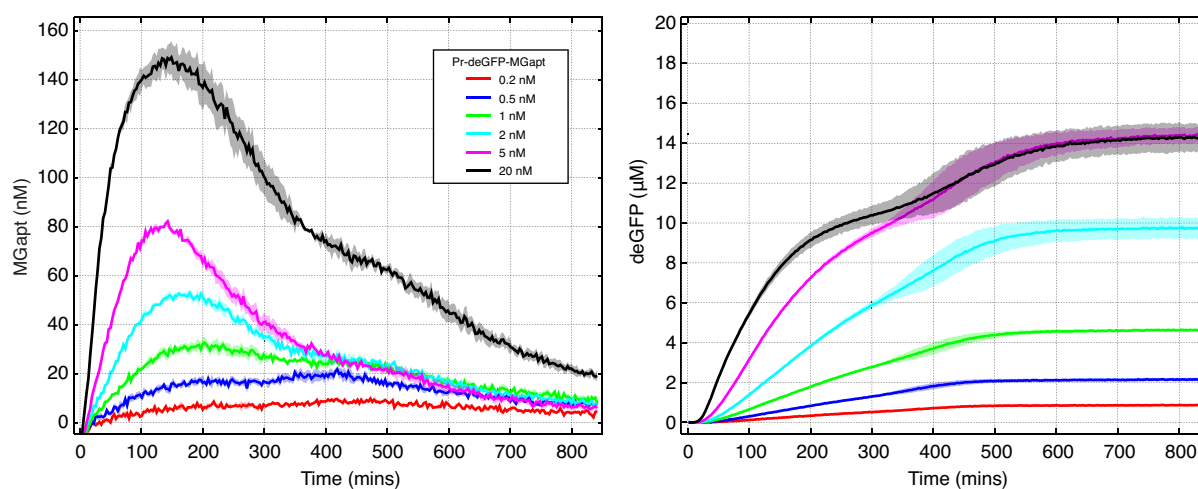


Figure S8: MGapt (left) and deGFP (right) expression kinetics when breadboard is supplemented with 1.25 mM of each of the four NTPs. Shaded regions indicate standard error over replicates.

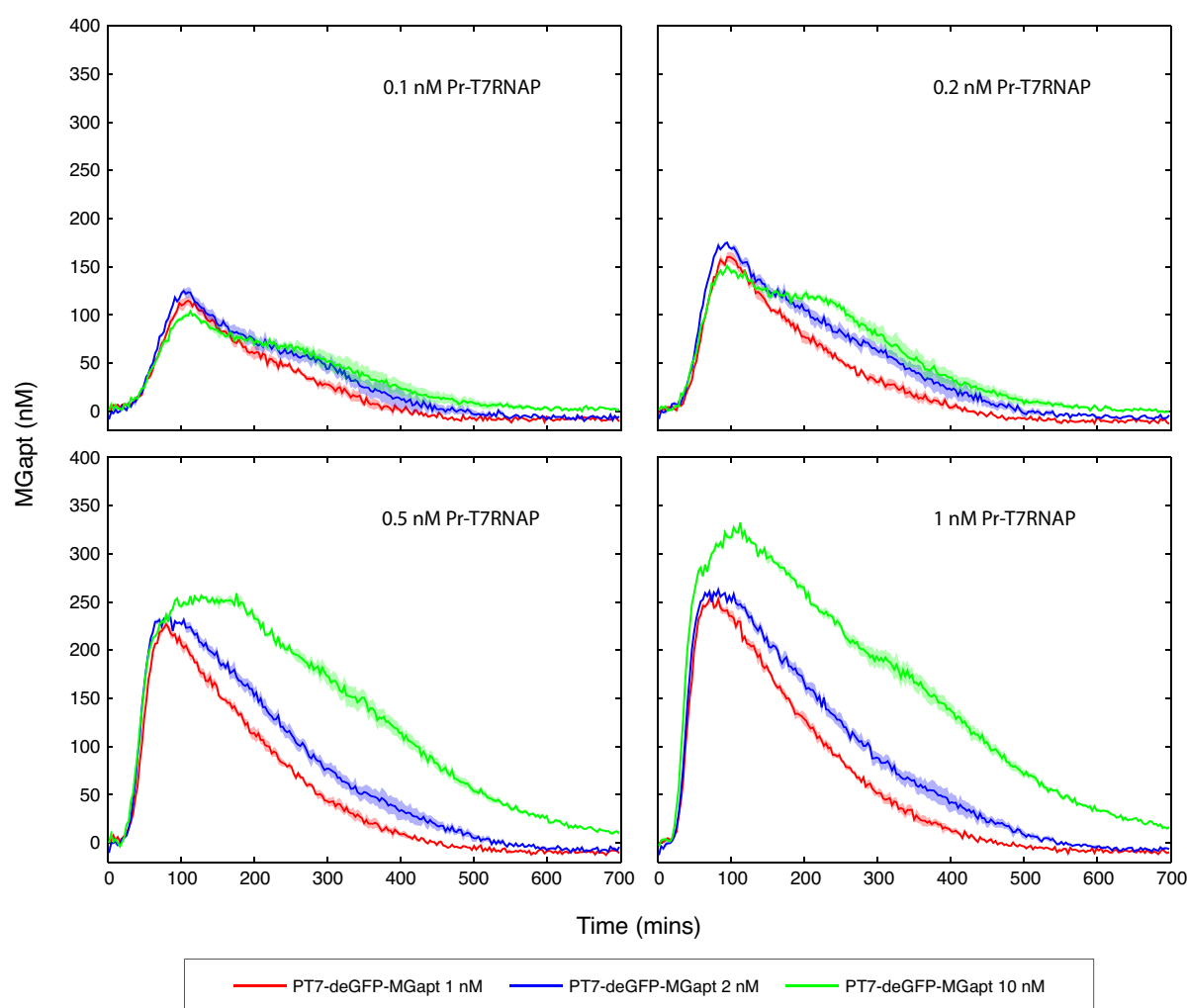


Figure S9: MGapt expression curves for T7 cascade tested with four different concentrations of first-stage T7 RNAP plasmid (0.1, 0.2, 0.5, and 1 nM Pr-T7 RNAP) and three different concentrations of the second-stage plasmid (1, 2, and 10 nM PT7-deGFP-MGapt). Shaded regions indicate standard error over replicates.

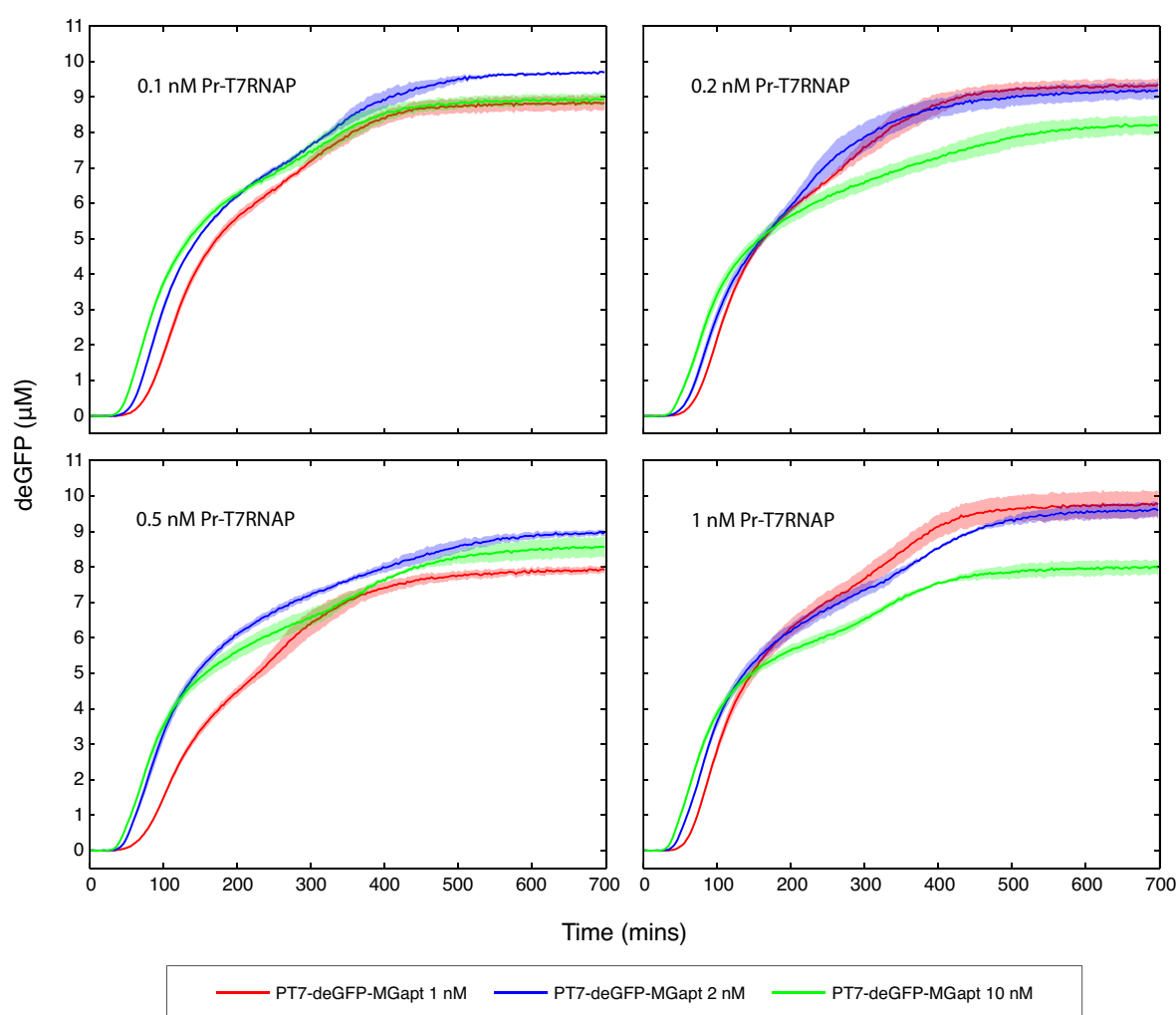


Figure S10: deGFP expression curves for T7 cascade tested with four different concentrations of the first-stage T7 RNAP plasmid (0.1, 0.2, 0.5, and 1 nM Pr-T7 RNAP) and three different concentrations of the second-stage plasmid (1, 2, and 10 nM PT7-deGFP-MGapt). Shaded regions indicate standard error over replicates.

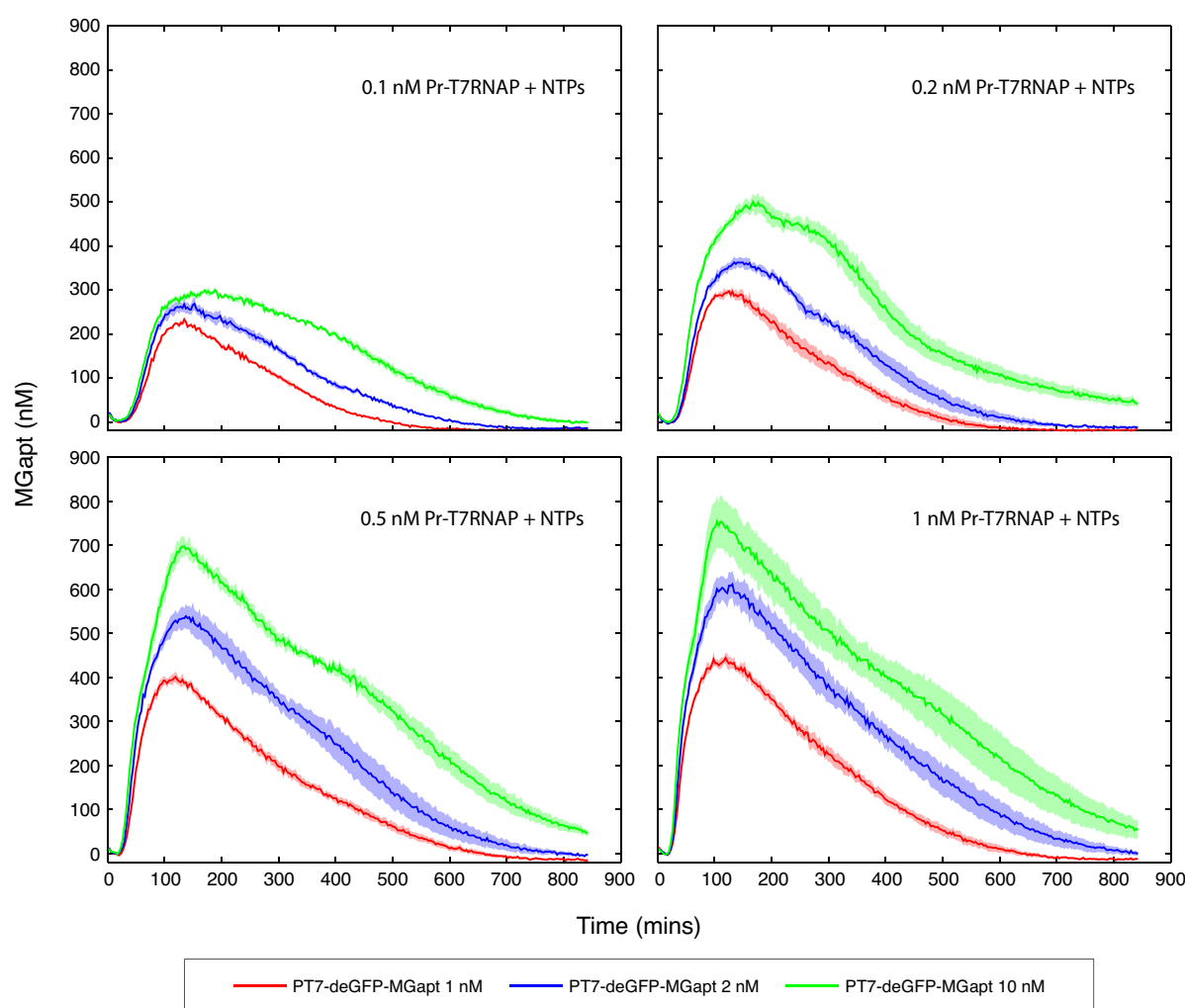


Figure S11: MGapt expression curves for T7 cascade tested with four different concentrations of first-stage T7 RNAP plasmid (0.1, 0.2, 0.5, and 1 nM Pr-T7 RNAP), three different concentrations of the second-stage plasmid (1, 2, and 10 nM PT7-deGFP-MGapt), and with the cell-free breadboard supplemented with 1.25 mM of each of the four NTPs. Shaded regions indicate standard error over replicates.

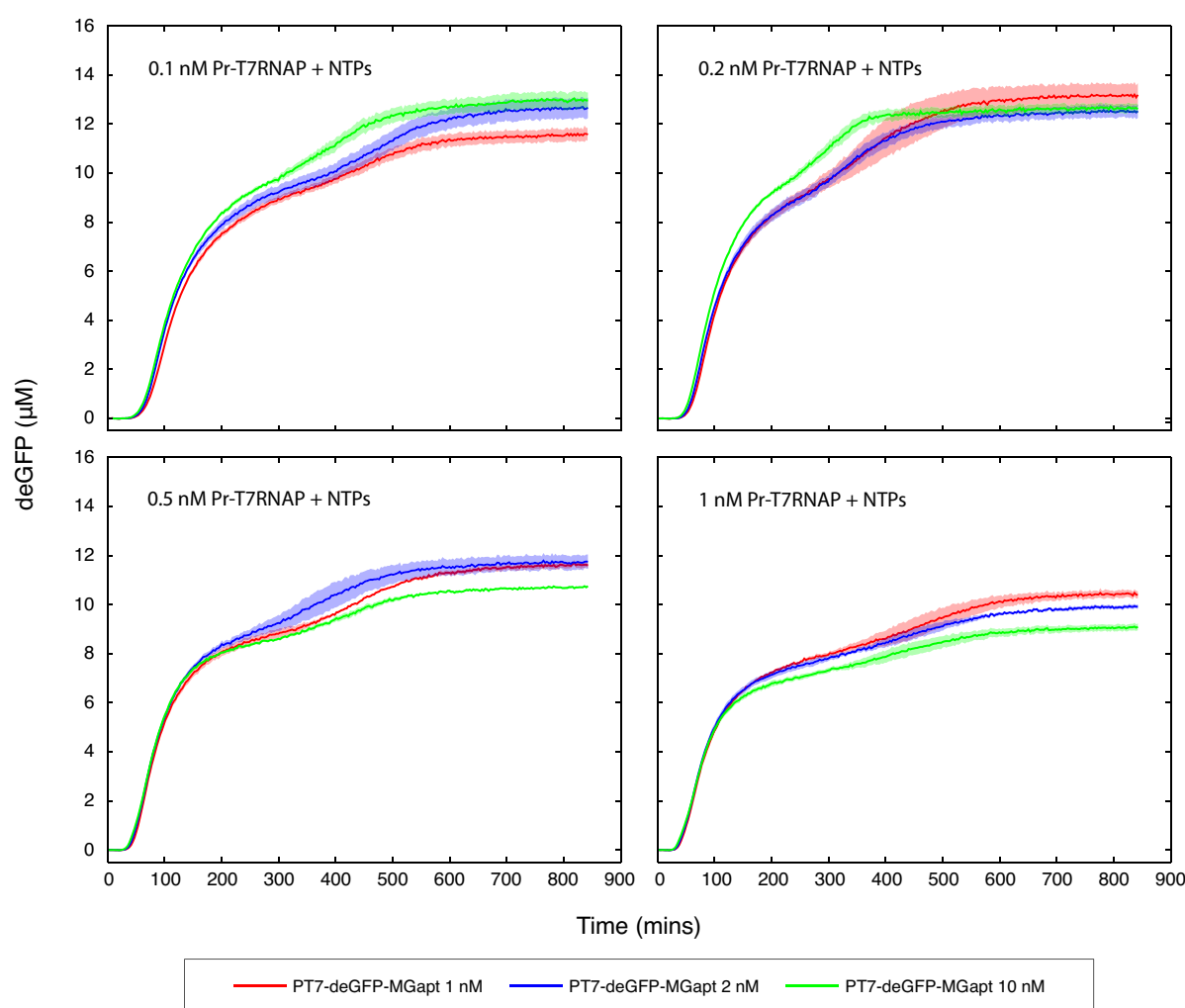


Figure S12: deGFP expression curves for T7 cascade tested with four different concentrations of the first-stage T7 RNAP plasmid (0.1, 0.2, 0.5, and 1 nM Pr-T7 RNAP), three different concentrations of the second-stage plasmid (1, 2, and 10 nM PT7-deGFP-MGapt), and with the cell-free breadboard supplemented with 1.25 mM of each of the four NTPs. Shaded regions indicate standard error over replicates.

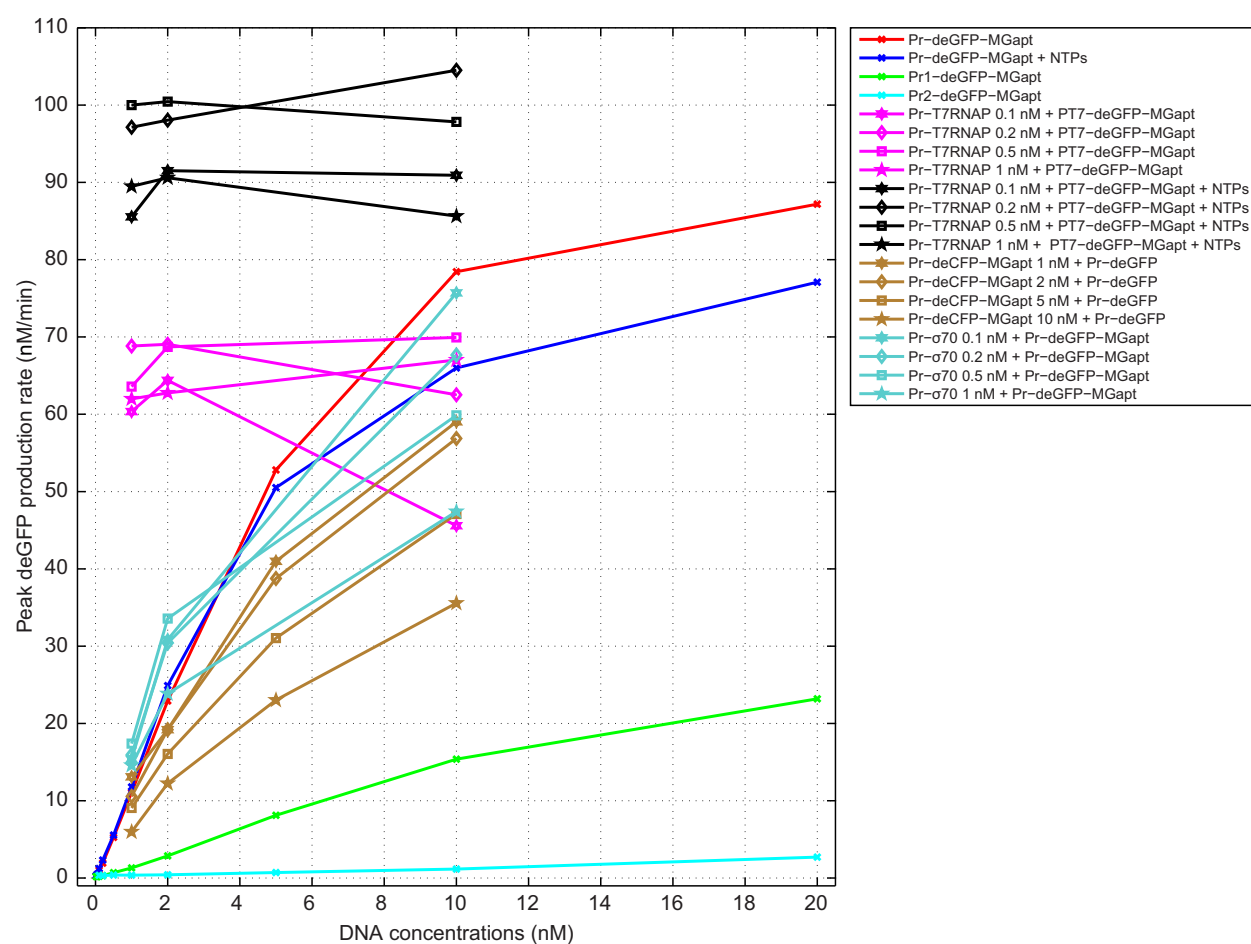


Figure S13: Maximum deGFP production rate as a function of reporter concentration under different conditions.

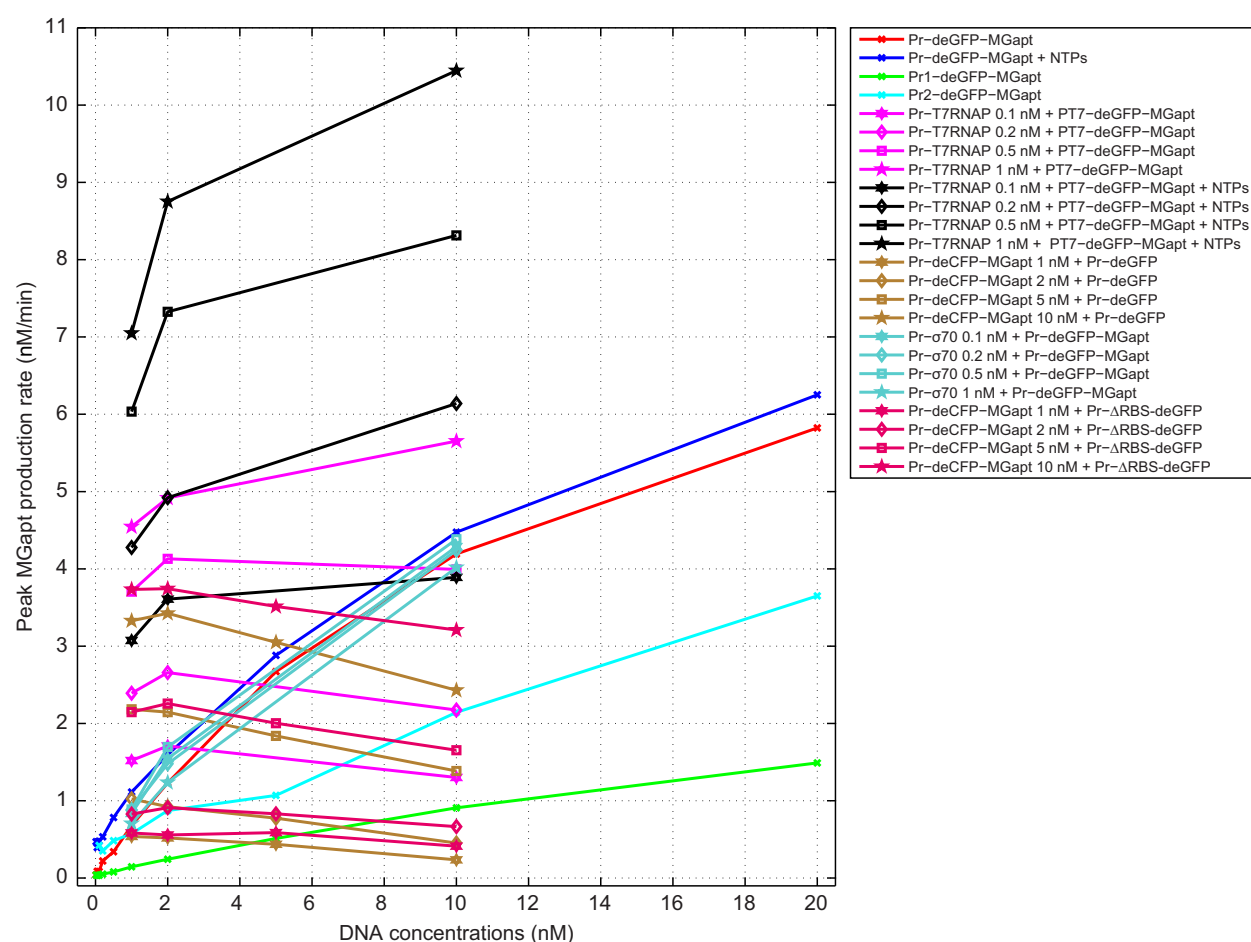


Figure S14: Maximum MGapt production rate as a function of reporter concentration under different conditions.

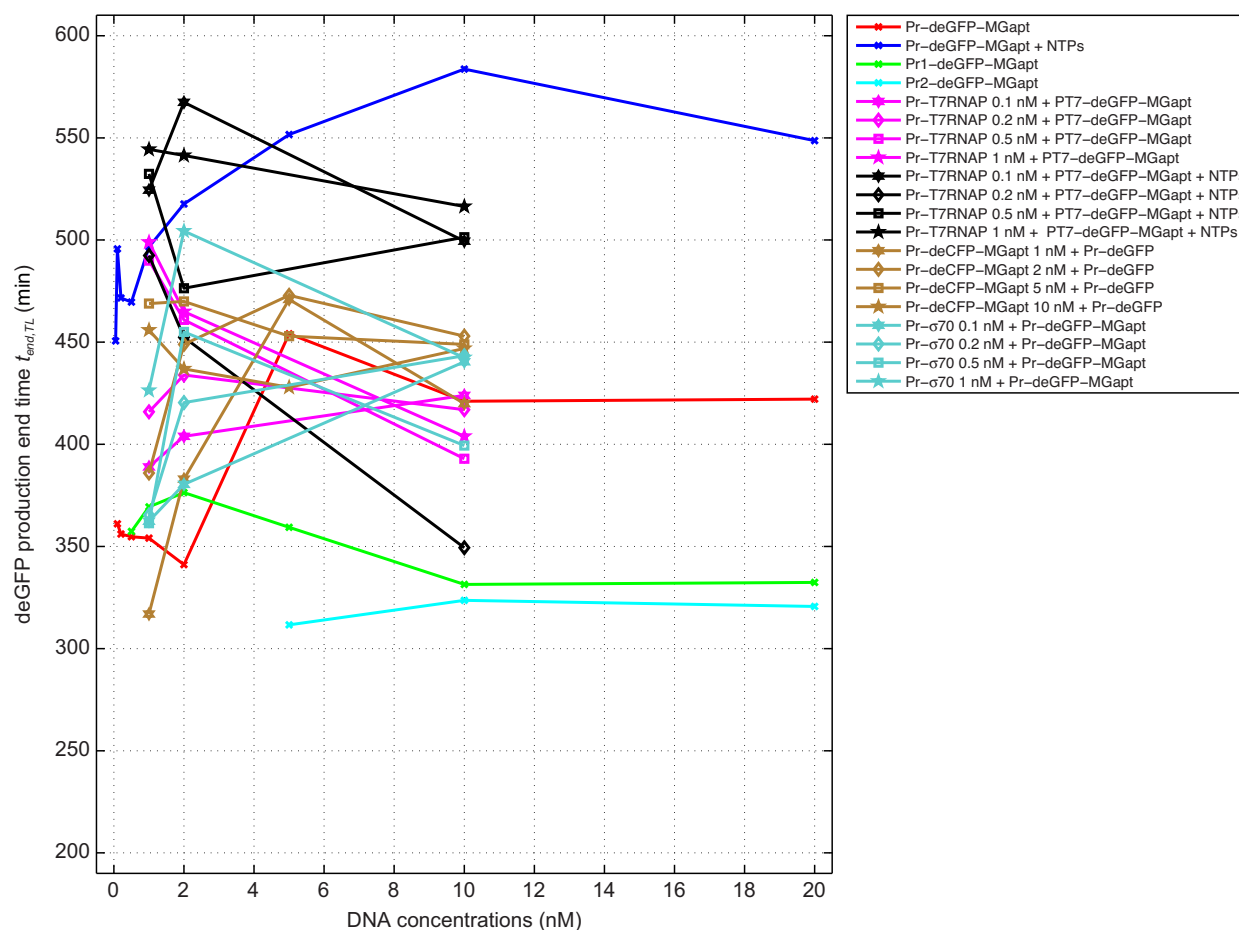


Figure S15: deGFP production end time $t_{end,TL}$, defined as the time at which the deGFP level reaches 95% of its final value (i.e., $\text{deGFP}(t_{end,TL}) = 95\% \times [\text{deGFP}]_{end}$).

Supplementary tables

Table S1: Genotypes of the plasmids used in this study.

Plasmid name	Transcription unit (TU)	TU size (bp)	Backbone/resistance
pBEST-Pr-GFP	P _R :deGFP:T500	810	ColE1/Amp ^R
pBEST-Pr-ΔRBS-GFP	P _R :ΔRBS-deGFP:T500	775	ColE1/Amp ^R
pBEST-Pr-GFP-MG	P _R :deGFP-MGapt:T500	869	ColE1/Amp ^R
pBEST-Pr1-GFP-MG	P _{R1} :deGFP-MGapt:T500	869	ColE1/Amp ^R
pBEST-Pr2-GFP-MG	P _{R2} :deGFP-MGapt:T500	869	ColE1/Amp ^R
pBEST-Pr-CFP-MG	P _R :deCFP-MGapt:T500	869	ColE1/Amp ^R
pBEST-Pr-σ ₇₀	P _R :σ ₇₀ :T500	1974	ColE1/Amp ^R
pBEST-Pr-T7RNAP	P _R :T7 RNAP:T500	3032	ColE1/Amp ^R
pBEST-Pr1-T7RNAP	P _{R1} :T7 RNAP:T500	3032	ColE1/Amp ^R
pBEST-Pr2-T7RNAP	P _{R2} :T7 RNAP:T500	3032	ColE1/Amp ^R
pIVEX-pT7-GFP-MG	P _{T7} :deGFP-MGapt:T7term	939	ColE1/Amp ^R